A Facile Route to Synthesizing Functionalized Mesoporous SBA-15 Materials with Platelet Morphology and Short Mesochannels

Shih-Yuan Chen,[†] Chih-Yuan Tang,[‡] Wei-Tsung Chuang,[§] Jey-Jau Lee,[§] Yi-Ling Tsai,[†] Jerry C. C. Chan,[†] Ching-Yen Lin,[‡] Yu-Cheng Liu,[||] and Soofin Cheng*,[†]

Department of Chemistry and Instrumental Center, National Taiwan University, Taipei 106, Taiwan, Research Division, National Synchrotron Radiation Research Center, Hsinchu 300, Taiwan, and Department of Raw Materials and Yarn Formation, Taiwan Textile Research Institute, Taipei County 236, Taiwan

Received December 8, 2007. Revised Manuscript Received February 29, 2008

A facile synthesis route for preparing SBA-15 silica of platelet shape and very short mesochannels (150−350 nm) was developed by introducing a small amount of Zr(IV) ions in the synthesis solution. The synthesis route can be easily extended to prepare platelet SBA-15 materials with various organic functional groups up to 1.87 mmol/g loading in one pot. In situ XRD and freeze-fracture replication TEM were found to be powerful techniques for studying the self-assembly processes. The platelet SBA-15 with short mesochannels in 150−350 nm was formed because of the fast self-assembly rate of P123 micelles and TEOS accelerated by the Zr(IV) ions in the synthesis solution. The platelet SBA-15 materials are superior to the conventional SBA-15 of rod or fiber morphologies in facilitating molecular diffusion and less possibility of pore blockage when used in the sorption or reactions of bulky molecules.

Introduction

Mesoporous silica materials of high surface areas and well-ordered pore structures have potential applications in separation, catalysis, microelectronic device, and enzyme immobilization.[1–4] SBA-15 material of two-dimensional channeling pores arranged in hexagonal *p6mm* structure has received great attention because of its relatively large pore and high hydrothermal stability in comparison to MCM-41, its analog in M41S family.[5,6] The diameter of the channeling pores of SBA-15 can be varied in 3−10 nm, whereas the length is usually in the scale of micrometers. Molecular diffusion through the lengthy mesochannels and pore blockage along the channels are the main concern when applying these materials for sorption and catalysis. Several papers have unveiled the preparation of pure siliceous SBA-15 materials with short mesochannels in the submicrometer level by adding either cosurfactant, cosolvent, electrolytes, or organosilanes into the synthesis solutions.[7–17] For example, Han and Ying[13] have reduced the particle size of mesoporous silica to 50−300 nm under a weak acidic synthesis condition using a mixture of triblock copolymer and cationic fluorocarbon surfactant. In other cases, NH_4F was added in addition to a cosolvent such as decane or octane to synthesize siliceous SBA-15 of cuboid or flake morphology with mesochannels in submicrometers.[9,14] The cosolvents and fluorocarbon surfactant were proposed to surround the silica particles and thereby limited the aggregation and growth of silica particles. However, these methods may not be ap-

* Corresponding author. Fax: 886-2-23636359. Tel: 886-2-33661662. E-mail: chem1031@ntu.edu.tw.
[†] Department of Chemistry, National Taiwan University.
[‡] Instrumental Center, National Taiwan University.
[§] National Synchrotron Radiation Research Center.
[||] Taiwan Textile Research Institute.

(1) (a) Feng, X.; Fryxell, G. E.; Wang, L. Q.; Kim, A. Y.; Liu, J.; Kemner, K. M. *Science* **1997**, *276*, 92. (b) Brown, J.; Mercier, L.; Pinnavaia, T. J. *Chem. Commun.* **1999**, 69.
(2) (a) Corma, A. *Chem. Rev.* **1997**, *97*, 237. (b) Wang, X.; Chen, C. C.; Chen, S. Y.; Mou, Y.; Cheng, S. *Appl. Catal., A* **2005**, *281*, 47. (c) Crudden, C. M.; Sateesh, M.; Lewis, R. *J. Am. Chem. Soc.* **2005**, *127*, 10045.
(3) (a) Baskaran, S.; Liu, J.; Domansky, K.; Kohler, N.; Li, X.; Coyle, C.; Fryxell, G. E.; Thevuthasan, S.; Williford, R. E. *Adv. Mater.* **2000**, *12*, 291. (b) Wang, Y.; Yang, C. M.; Schmidt, W.; Spliethoff, B.; Bill, E.; Schüth, F. *Adv. Mater.* **2005**, 17. (c) Yang, P. D.; Wirnsberger, G.; Huang, H. C.; Cordero, S. R.; McGehee, M. D.; Scott, B.; Deng, T.; Whitesides, G. M.; Chmelka, B. F.; Buratto, S. K.; Stucky, G. D. *Science* **2000**, *287*, 465.
(4) (a) Lu, A. H.; Schuth, F. *C. R. Chim.* **2005**, *8*, 609. (b) Han, Y.; Lee, S. S.; Ying, J. Y. *Chem. Mater.* **2006**, *18*, 643. (c) Tian, R.; Zhang, H.; Ye, M.; Jiang, X.; Hu, L.; Li, X.; Bao, X.; Zou, H. *Angew. Chem., Int. Ed.* **2007**, *46*, 962.
(5) (a) Kresge, C. T.; Leonowicz, M. E.; Roth, W. J.; Vartuli, J. C.; Beck, J. S. *Nature* **1992**, *359*, 710. (b) Beck, J. S.; Vartuli, J. C.; Roth, W. J.; Leonowicz, M. E.; Kresge, C. T.; Schmitt, K. D.; Chu, C. T.-W.; Olson, D. H.; Sheppard, E. W.; McCullen, S. B.; Higgins, J. B.; Schlenker, J. L. *J. Am. Chem. Soc.* **1992**, *114*, 10834.
(6) (a) Zhao, D.; Feng, J.; Huo, Q.; Melosh, N.; Fredrickson, G. H.; Chmelka, B. F.; Stucky, G. D. *Science* **1998**, *179*, 548. (b) Zhao, D.; Huo, Q.; Feng, J.; Chmelka, B. F.; Stucky, G. D. *J. Am. Soc. Chem.* **1998**, *120*, 6024.
(7) Konya, Z.; Zhu, J.; Szegedi, A.; Kiricsi, I.; Alivisatos, P.; Somorjai, G. A. *Chem. Commun.* **2003**, 314.
(8) Fan, J.; Lei, J.; Wang, L.; Yu, C.; Tu, B.; Zhao, D. *Chem. Commun.* **2003**, 2140.
(9) Zhang, H.; Sun, J.; Ma, D.; Bao, X.; Klein-Hoffmann, A.; Weinberg, G.; Su, D.; Schlogl, R. *J. Am. Chem. Soc.* **2004**, *126*, 7440.
(10) Chen, S. Y.; Jang, L. Y.; Cheng, S. *Chem. Mater.* **2004**, *16*, 4174.
(11) Chen, B.-C.; Lin, H.-P.; Chao, M.-C.; Mou, C.-Y.; Tang, C.-Y. *Adv. Mater.* **2004**, *16*, 1657.
(12) Shan, W.; Wang, B.; Zhang, Y.; Tang, Y. *Chem. Commun.* **2005**, 1877.
(13) Han, Y.; Ying, J. Y. *Angew. Chem., Int. Ed.* **2005**, *44*, 288.
(14) Sun, J. M.; Zhang, H.; Tian, R. J.; Ma, D.; Bao, X. H.; Su, D. S.; Zou, H. F. *Chem. Commun.* **2006**, 1322.
(15) Sujandi.Park, S. E.; Han, D. S.; Han, S. C.; Jin, M. J.; Ohsuna, T. *Chem. Commun.* **2006**, 4131.
(16) Cui, X.; Moon, S.-W.; Zin, W.-C. *Mater. Lett.* **2006**, *60*, 3857.
(17) Kipkemboi, P.; Fogden, A.; Alfredsson, V.; Flodstrom, K. *Langmuir* **2001**, *17*, 5398.

10.1021/cm703500c CCC: $40.75
Published on Web 05/20/2008

plicable to prepare organic functionalized materials in one pot because of the interference of the cosolvents in the self-assembly process and the reactivity of NH_4F toward organosilanes. Among the literature up to now, only one of them described the preparation of amino-functionalized mesoporous SBA-15.[15] Nevertheless, the method was limited to preparing SBA-15 silica with a narrow amino-loading. The incorporation of organic functional groups is important in the applications of mesoporous silica. Here, we report a facile synthesis route for preparing SBA-15 silica of platelet shape and very short mesochannels (150−350 nm). Moreover, the synthesis route can be easily extended to prepare platelet SBA-15 materials with various organic functional groups up to 1.87 mmol/g loading in one pot. The self-assembly processes were examined by the in situ XRD and freeze-fracture replication TEM techniques. The advantages of the resultant materials were demonstrated by the faster adsorption rates and larger adsorption capabilities toward bulky organic molecules, in comparison to the conventional SBA-15.

Experimental Methods

Synthesis. Conventional SBA-15 of rod-shape was prepared by dissolving 1.00 g of Pluronic P123 triblock copolymer (Aldrich, $M_n = 5800$) in 40.0 g of 2 M HCl solution at 35 °C, followed by adding 2.10 g of TEOS (Acros 98%). The reactant compositions were 0.017:1:7.94:221 P123:TEOS:HCl:H_2O. The mixture was sealed in a polypropylene bottle, stirred at 35 °C for 24 h, and then hydrothermally heated at 90 °C under static conditions for another 24 h. The solid product was filtered, washed with deionized water, and dried at 50 °C overnight. The P123 templates were removed by calcining the material at 500 °C in air for 12 h with a ramping rate of 1 °C/min. Platelet SBA-15 was prepared by adding a small amount of Zr(IV) ions in the conventional SBA-15 synthesis solution. The reactant compositions were 0.017:1:0.03−0.1:7.94:221 P123:TEOS:$ZrOCl_2 \cdot 8H_2O$:HCl:H_2O.

Platelet SBA-15 materials functionalized with 5−30 mol% organic functional groups were prepared by one-pot method. Prior to the addition of the organosilane, TEOS was prehydrolyzed in the synthesis solution containing HCl, P123 and Zr(IV) ions for 1−4 h. P123 was removed by ethanol extraction at 78 °C for 1 day.

Adsorption. The adsorption of new coccine (Arcos, $C_{20}H_{11}N_2Na_3O_{10}S_3$, MW = 604.5 g/mol) was carried out by adding 50 mg of the solid in 10 mL of new coccine solution (0.0385 mM) under stirring at room temperature. After various periods, the solid was separated from the solution by filtration and the concentration of new coccine in the filtrate was determined by absorbance at 507 nm.

Characterization. XRD patterns were recorded using a PANalytical diffractometer with $Cu_{K\alpha}$ radiation operated at 40 mA and 45 kV. The textural properties of samples were analyzed by nitrogen physical adsorption at liquid N_2 temperature (77 K) using a Micromeritics Tristar 3000 instrument. Prior to the experiments, the samples were degassed at 120 °C for more than 8 h under a vacuum (1×10^{-3} Torr). The specific surface areas were evaluated using Brunauer−Emmett−Teller (BET) method in the P/P_0 range of 0.05−0.3. Pore size distribution curves were calculated using the desorption branch of the isotherms and the Barrett−Joyner−Halenda (BJH) method[18] and pore sizes were obtained from the peak positions of the distribution curves. The elemental contents in bulk were determined by inductive-coupled plasma-atomic emission spectroscopy (ICP-AES, ELAN 5000 instrument). The elemental analysis of C, H, N, and S was measured by using a Heraeus VarioEL analyzer. The in situ XRD experiments were carried out at Beam line 17A of National Synchrotron Radiation Center (NSRRC) at Hsinchu, Taiwan. The wavelength of the X-ray source was 1.334431 Å. The gelled sample was pumped into a Teflon sample cell by using wriggle pump. The in situ XRD patterns were collected every 3 min using image plate detection. The TEM images of freeze-fracture replication (FFR) were performed using a Hitachi H-7100 Transmission Electron Microscope operating at 75 kV. The liquid sample was dropped in between two electron microscopy gold grids. The sandwiched sample was then frozen at liquid N_2 temperature. The frozen sandwich was split in a Balzers freeze-fracture apparatus (BAF 400 D) and coated with a Pt−C thin layer at 45° angle, followed by coating another carbon layer at 90°. The replicas were received by throwing the coated sample in a HF solution. The scanning electron microscopy (SEM) images and energy-dispersed X-ray spectrometer (EDX) were taken on a Hitachi S-800 field-emission scanning electron microscope and S-2400 scanning electron microscope, respectively. The NMR experiments were carried out at ^{29}Si,^{13}C, and ^{1}H frequencies of 59.6, 75.5, and 300.1 MHz, respectively, on a Bruker DSX300 NMR spectrometer equipped with a commercial 7 mm MAS NMR probe with magic-angle spinning (MAS) frequencies setting at 5 kHz for all experiments. The chemical shifts were externally referred to tetramethylsilane for ^{29}Si and ^{13}C. For the ^{29}Si Bloch-decay experiment, the recycle delay was set to 60 s. The $Q_4/(Q_2+Q_3)$ area ratios were obtained by deconvolution of the peaks in the spectra using WinFit software. $^{13}C\{^1H\}$ cross-polarization spectra were measured with a recycle delay of 4 s, and the contact times were 1.5 ms. During the contact time the ^{1}H nutation frequency was set equal to 50 kHz, and a linear ramping was applied to the nutation frequencies of ^{13}C (27.3−43.0 kHz). The proton decoupling field during the acquisition period was 83 kHz.

Results and Discussion

The platelet SBA-15 materials were prepared by adding small amounts of Zr(IV) ions (Zr/Si = 0.03−0.1) in the conventional SBA-15 synthesis solutions. The optimal molar compositions in the synthesis solution were 0.017:1:0.05:7.94:221 P123:TEOS:$ZrOCl_2 \cdot 8H_2O$:HCl:H_2O. Figure 1 shows the resultant siliceous SBA-15 has three distinct diffraction peaks at $2\theta = 0.90$, 1.52, and 1.76° indexed to the (100), (110), and (200) planes, respectively, of 2D hexagonal *p6mm* symmetry[6] and a narrow pore size distribution with the peak pore diameter at 6.7 nm. SEM photograph shows the materials are homogeneously dispersed hexagonal thin platelets. The average width and thickness of the platelets are 800−1100 nm and 150−300 nm, respectively. Well-ordered pores arranged in 2D hexagonal *p6mm* structure and aligned along the thickness of the thin platelets are observed on the TEM photographs. In other words, the lengths of mesochannels are the thickness of the thin platelets, which are slightly thinner at the edge and thicker at the center. The platelet morphology and short mesochannels of these materials are quite different from those of conventional SBA-15, which possesses rod- or fiberlike morphology and long mesochannels in micrometers (see the Supporting Information).[6]

(18) Wang, X.; Lin, K. S. K.; Chan, J. C. C.; Cheng, S. *J. Phys. Chem. B* **2005**, *109*, 1763.

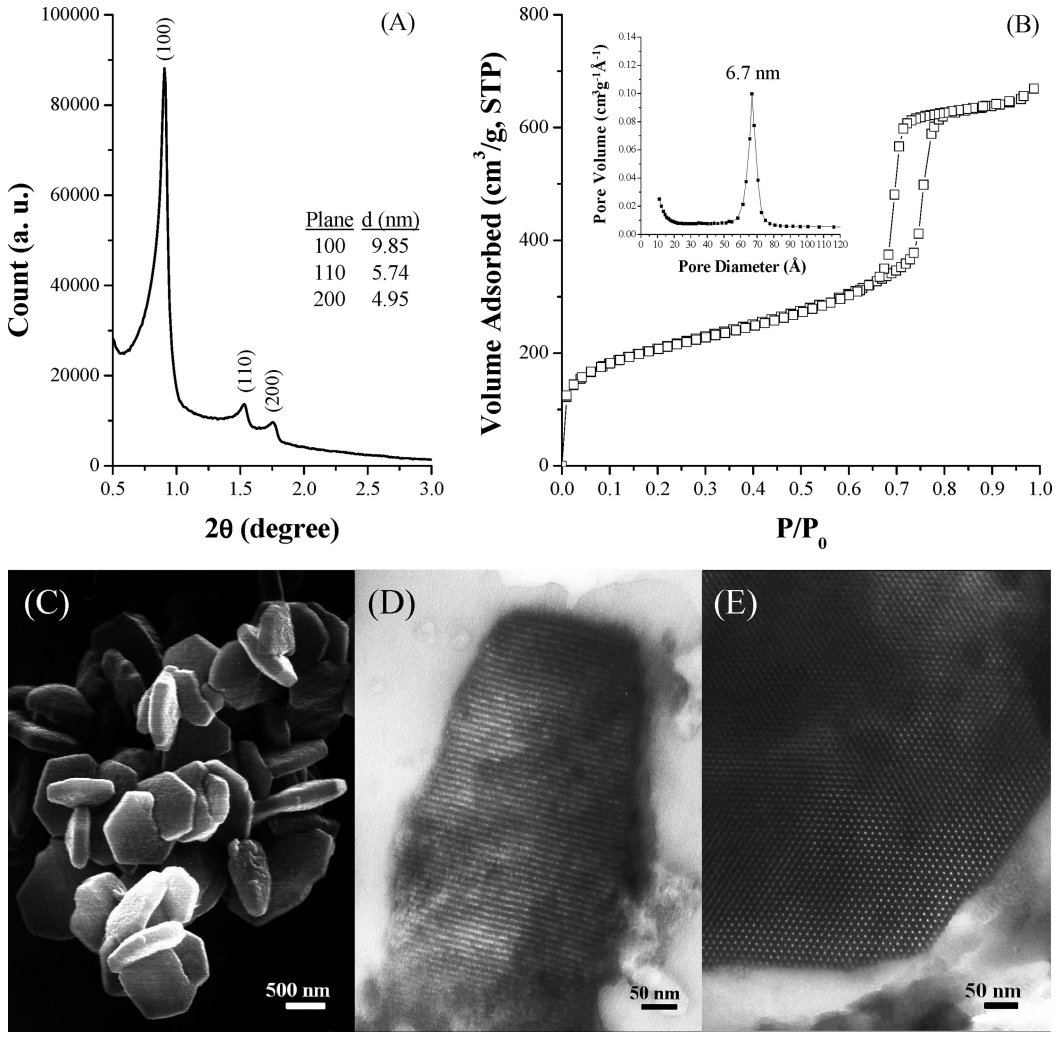

Figure 1. (A) Small-angle XRD pattern using $Cu_{K\alpha}$ radiation source ($\lambda = 1.5418$ Å), (B) N_2 sorption isotherm, (C) SEM image, and (D, E) TEM images of calcined SBA-15 with platelet morphology and short mesochannels.

This new synthesis route could be easily extended to prepare organic functionalized SBA-15. Figure 2 shows the small-angle XRD patterns of the resultant SBA-15 materials with various organic functionalities, including CH_3, Ph, $Cl(CH_2)_3$, $SH(CH_2)_3$, $CN(CH_2)_3$, and $NH_2(CH_2)_3$ groups. Three distinct diffraction peaks indexed to the (100), (110), and (200) planes of 2D hexagonal *p6mm* symmetry appear at $2\theta \approx 0.7-2°$. The positions of the diffraction peaks vary slightly for materials containing different organic groups, implying that the aggregation numbers of P123 micelles are affected by the organosilane precursors.

Figure 3 shows the EM photographs of the organic functionalized SBA-15. All the materials are still homogeneously dispersed hexagonal thin platelets. The thickness of the platelets of the functionalized SBA-15 is slightly thicker than that of pure siliceous SBA-15, but the channeling pores are still aligned along the height of the platelets (see the Supporting Information). The average thickness of the platelets are in 150−350 nm.

The N_2 sorption isotherms of the ethanol extracted platelet SBA-15 materials show the classical type IV isotherms with H_1 hysteresis loops appeared at $P/P_0 \approx 0.5-0.8$, depending on the functional groups (abbreviated as FG). The derived textural properties are shown in Table 1. All the materials possess high surface area (611−810 m^2/g), large pore volume (0.57−1.01 cm^3/g), thick pore wall (4.6−7.1 nm), and large mesopores (4.2−6.7 nm) with narrow pore size distribution (PSD < 1.4 nm), similar to those of conventional SBA-15 material.[6] Moreover, the organic functionalized SBA-15 materials have smaller pore diameters but thicker pore walls than those of siliceous SBA-15, implying that the organic functional groups should be incorporated onto the silica framework. On the other hand, the pore diameters of the organic functionalized SBA-15 platelets vary with different organic groups, indicating that the aggregation numbers of P123 micelles are changed by the organic moieties of organosilanes.

It is also noticeable that the pore diameter of siliceous platelet SBA-15 is slightly larger than those of conventional siliceous fiber-shaped SBA-15, revealing that the average micellar radius of P123 micelles was increased in the presence of Zr(IV) ions. It is attributed to the so-called salting out effect that the hydrophobic core of P123 micelle is expanded as the hydrophilicity of the PEO chains decreases.[19] As a result, the micropore area and volume determined by nitrogen physisorption are 202 m^2/g and 0.091

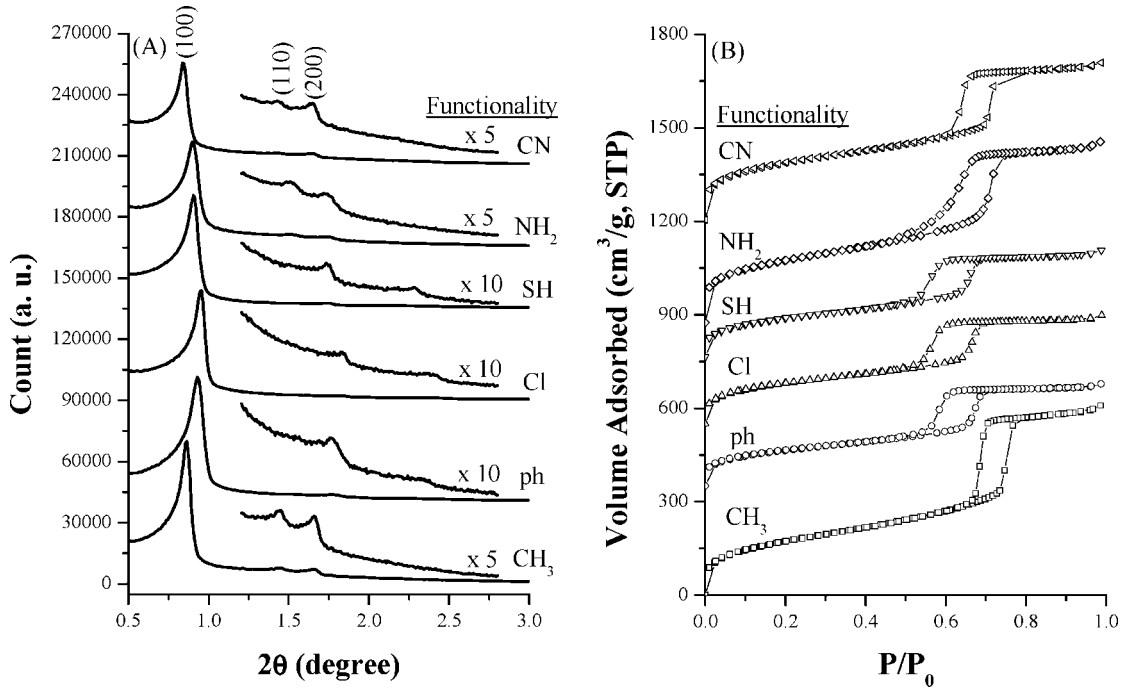

Figure 2. (A) Small-angle XRD patterns using $Cu_{K\alpha}$radiation source ($\lambda = 1.5418$ Å), (B) N_2 sorption isotherms of extracted organic functionalized SBA-15 with platelet morphology and short mesochannels.

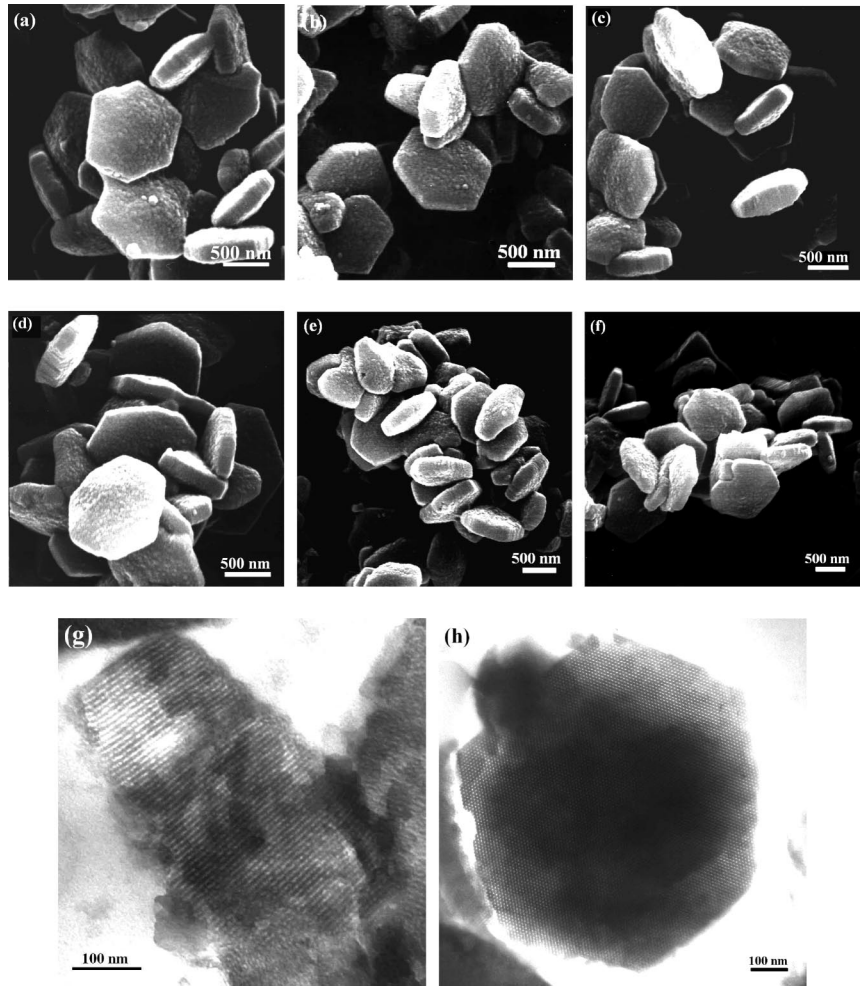

Figure 3. SEM and selected TEM images of various extracted organic functionalized SBA-15 with platelike morphology and short mesochannels (a) CH_3, (b) Ph, (c) Cl, (d, g, h) SH, (e) NH_2, (f) CN.

Table 1. Elemental Analyses and Textural Properties of Extracted Organic Functionalized SBA-15 Platelets with Short Mesochannels

functionality	PT[a](h)	FG/Si gel	FG/Si solid[b]	a_0(nm)	S_{BET}(m^2/g)	V_{Total}(cm^3/g)	Φ_P[c](nm)	PSD[d](nm)	W[e](nm)
none	0	0.091	0.034	11.3	732	1.01	6.7	0.8	4.6
CH_3	1	0.091	0.096	11.9	810	1.00	6.4	0.8	5.2
Ph	2	0.091	0.100	11.0	662	0.71	4.5	1.1	6.5
$(CH_2)_3Cl$	2	0.091	0.099	10.7	611	0.57	4.5	1.1	6.2
$(CH_2)_3SH$	2	0.091	0.086	11.3	616	0.57	4.2	1.2	7.1
$(CH_2)_3NH_2$	4	0.091	0.088	11.4	712	0.87	5.4	1.4	6.0
$(CH_2)_3CN$	1	0.091	0.100	12.2	744	0.82	5.5	1.2	6.7

[a] Prehydrolysis period. [b] FG/Si molar ratios are measured by CHNS elemental analysis. [c] Pore diameter. [d] Pore size distribution. [e] Wall thickness.

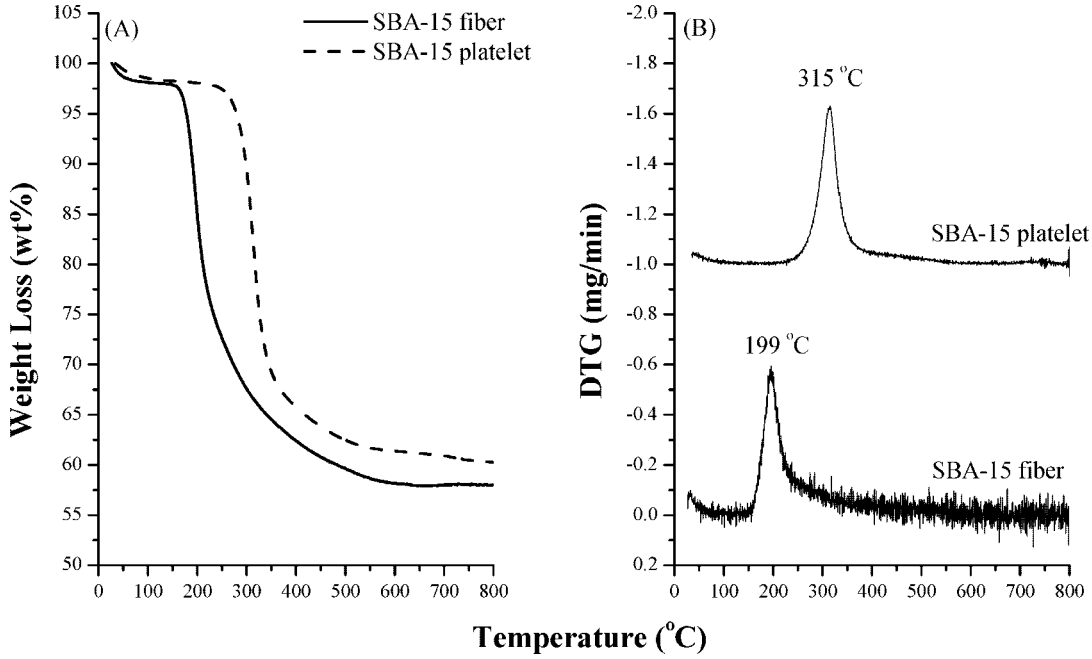

Figure 4. (A) TG and (B) DTG profiles of as-made SBA-15 materials with conventional fiberlike and platelet morphologies.

cm^3/g, respectively, for siliceous fiber-shaped SBA-15, while those are lowered to 159 m^2/g and 0.070 cm^3/g, respectively, for the platelet SBA-15 synthesized with Zr(IV) ions.

The interaction between P-123 template and the silica framework was examined by thermal analysis (Figure 4). For conventional fiber-shaped SBA-15, a steep weight loss appeared at 170−290 °C is attributed to the decomposition of P123 triblock copolymer.[6] For platelet-shaped SBA-15, the weight loss shifts to 240−380 °C, implying that the interaction between P123 and silica framework is stronger when Zr(IV) ions are present. On the other hand, the Zr/Si atomic ratio analyzed by surface sensitive EDX technique was 0.043 and higher than that by ICP-AES (Zr/Si = 0.034). These results infer that the Zr(IV) species are probably present on the surface of the silica wall and bind strongly to P123 micelles.

The in situ XRD technique was utilized to study the effect of Zr(IV) ions on the self-assembly of P123 micelles and silica precursors by using Sychrotron X-ray source at beam line 17A of NSRRC, Taiwan.[20a] For the conventional SBA-15 with fiberlike morphology, the gel compositions were 0.017:1.0:7.94:221 P123:TEOS:HCl:H_2O.[6] Figure 5a shows that a broad diffraction peak at $2\theta = 0.66°$ corresponding to d-spacing of 13.4 nm appeared after TEOS was added for 52.2 min. Meanwhile, white precipitate was observed. Higher-angle diffraction peaks of (110) and (200) planes gradually appeared after about 2 h. These results were similar to those in previous reports.[20b,c] For the SBA-15 prepared with Zr(IV) ions, a diffraction peak at $2\theta = 0.61°$ corresponding to d-spacing of 14.5 nm was promptly observed after TEOS was added for 7.3 min (Figure 5b). The white precipitate was also seen at this moment. The (110) and (200) diffraction peaks appeared after about 30 min. The effect of Zr/Si ratio on the time needed for the first appearance of diffreaction peak (designated as τ) is shown in Figure 5c. The τ drops markedly from 52 min to ca. 20 min by adding only 2.5 mM of $ZrOCl_2$ in the synthesis solution. With a further increase in the Zr(IV) concentration, the τ value decreases gradually and lowers to ca. 7 min when 12.5 mM of $ZrOCl_2$ is added. These results demonstrate that the formation of ordered mesoporus silica is accelerated by Zr(IV) ions.

The aggregation of P123 micelles in the synthesis solution before and after the addition of TEOS was studied

(19) (a) Kabalnov, A.; Olsson, U.; Wennerstron, H. *J. Phys. Chem.* **1995**, *99*, 6220. (b) Alfredsson, V.; Amenitsch, H.; Kleitz, F.; Linden, M.; Linton, P.; Teixeira, C. V. *Stud. Surf. Sci. Catal.* **2005**, *158*, 97. (c) Li, C.; Wang, Y.; Guo, Y.; Liu, X.; Guo, Y.; Zhang, Z.; Wang, Y.; Lu, G. *Chem. Mater.* **2007**, *19*, 173.

(20) (a) Liu, M.-C.; Sheu, H.-S.; Cheng, S. *Chem. Commun.* **2002**, 854. (b) Flodstrom, K.; Teixeira, C. V.; Amenitsch, H.; Alfredsson, V.; Linden, M. *Langmuir* **2004**, *20*, 4885. (c) Flodstrom, K.; Wennerstrom, H.; Teixeira, C. V.; Amenitsch, H.; Linden, M.; Alfredsson, V. *Langmuir* **2004**, *20*, 10311.

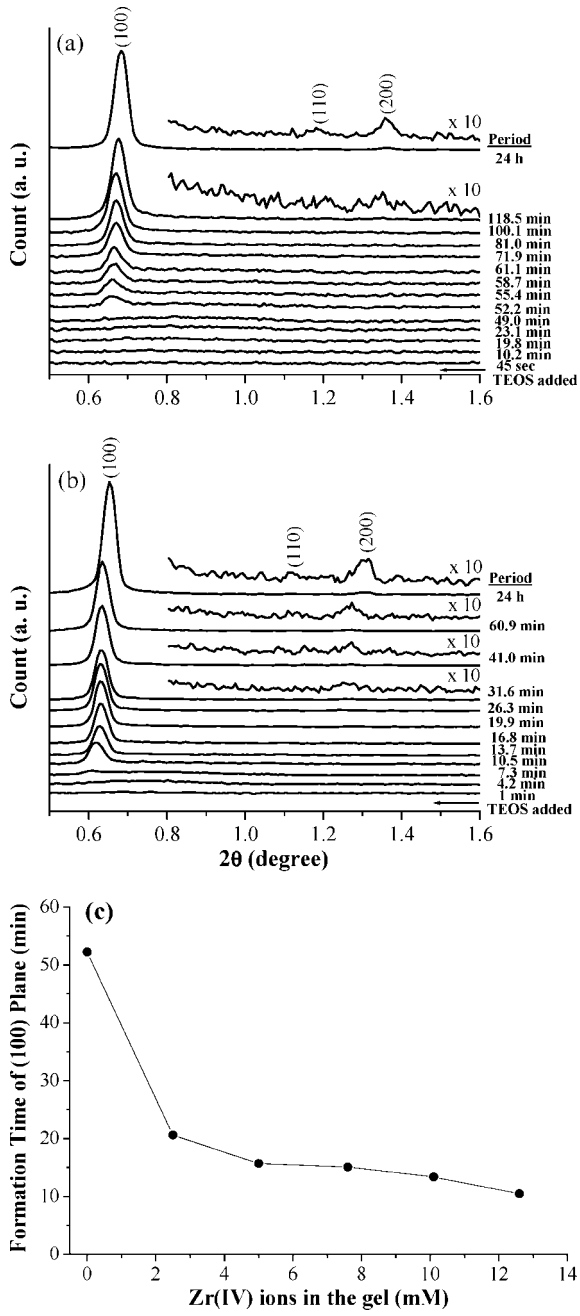

Figure 5. In situ XRD patterns using a synchrotron X-ray radiation source ($\lambda = 1.33344$ Å) of SBA-15 prepared (a) without adding Zr(IV) ions, (b) with Zr(IV) ions, and (c) the effect of Zr(IV) concentration on the time (τ) of first appearance of the diffraction peak.

by TEM microscopy. No mesophase of P123 micelles could be detected in the P123−HCl−H_2O synthesis solution prior to the addition of TEOS. Because the P123 concentration in the solution was 2.5 wt % and much higher than the critical micellar concentration (cmc) of P123 molecules (0.025 wt % at 25 °C),[21] this result infers that the electron density of P123 micelles is too low to be detected by the electron microscope. The aggregates of worm-like P123 micelles of ca. 4−6 nm in diameter became detectable only after TEOS was added. However, the aggregation number and the structure of the micelles could be changed during the drying process when preparing the specimens for TEM.

To avoid the possible interference from drying or the stain agent, we further monitored the self-assembly processes by directing the images of freeze-fracture replication (FFR) with TEM technique. The wet gels collected after various reaction periods were quenched immediately in liquid N_2 and the TEM photographs of the replicas were taken. Figure 6 shows that after TEOS was added for 30 min, aggregates in 800 nm−2 μm with ruptures and worm pores were seen. Further reaction for 1 h, no significant changes in the particle morphology and pore structure were observed. However, pronounced changes were seen after reaction for 1.5 h. The particles turn to short-rod morphology with a thickness in ca. 600 nm and diameter in 2 μm. In addition, some of the short rods are interconnected and form longer rods, and well-arranged mesochannels can be seen along the length of the short rods. Further prolonging the reaction to 3 h, the diameter of the rods does not change significantly but the length of the rod increases to micrometer level. It is mentionable that the structures and sizes of the replicas inevitably include the thicknesses of Pt−C and C coverages, which are about 2 and 20 nm, respectively.

In the synthesis solution containing Zr(IV) ions, the aggregates containing tinny cylinders of 25−50 nm in diameters dispersed in a linear pattern were observed after TEOS was added for 30 min (Figure 7). The short rods are likely a result of silica condensation around the threadlike P123 micelles. After another 10 min, platelike particles with ordered mesochannels aligned along the thickness of the platelets were seen. The diameters of the channeling pores were around 10.5 nm. The pore diameter shrank slightly to 8.5−9 nm due to further silica condensation as the reaction was prolonged. Clearly, the ordered porous structure appeared much faster than that without Zr(IV). It is also noticeable that no growth of the particles along the channeling direction was seen with the prolongation of the reaction.

Ruthstein and co-workers[21d] have observed spherical micelles of P123 by direct imaging cryo-TEM experiments after adding tetramethyl orthosilicate (TMOS) as silica source into the P123 solution containing H_3PO_4 for 6.5−8.5 min. After 22 min, spherically micelles of 9.7 ± 1 nm in average diameter and flexible threadlike micelles of 7.1 ± 0.9 nm in diameter and 15−30 nm in length were reported to coexist. In HCl, the apprearance of spherical and threadlike micelles has been shortened to 5.2 and 14.1 min, respectively. These results are attributed to that the weaker acidity of H_3PO_4 makes silica condensation in a slower rate and a relatively longer period is needed to observe the silica coated micelles. As the silica condensation further proceeded, the P123−silica nanocomposite was formed, which transformed gradually to 2D hexagonal arrangement. Again, it took 2 h in H_3PO_4, but only 22 min in HCl.

(21) (a) Flodstrom, K.; Wennerstrom, H.; Alfredsson, V. *Langmuir* **2004**, *20*, 680. (b) Linden, M.; Schunk, S. A.; Schuth, F. *Angew. Chem., Int. Ed.* **1998**, *37*, 6–821. (c) Ruthstein, S.; Frydman, V.; Kababya, S.; Landau, M.; Goldfarb, D. *J. Phys. Chem. B* **2003**, *107*, 1739. (d) Ruthstein, S.; Schmidt, J.; Kesselman, E.; Talmon, Y.; Goldfarb, D. *J. Am. Chem. Soc.* **2006**, *128*, 3366.

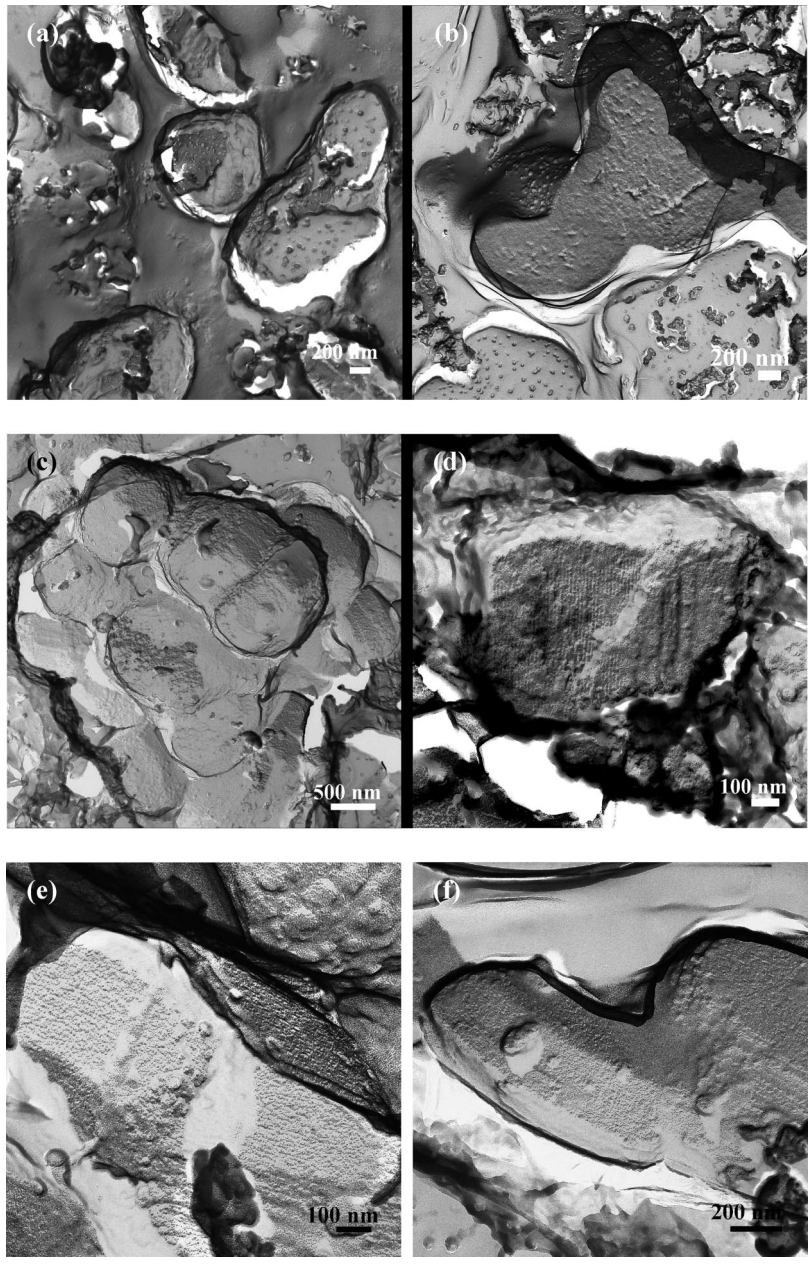

Figure 6. Freeze-fracture replication TEM images of SBA-15 synthesis solution during conventional synthesis process, taken after adding TEOS for (a) 30 min, (b) 1 h, (c, d) 1.5 h, and (e, f) 3 h.

In combination with the results of cryo-TEM studies reported in the literature[21d] and present freeze-fracture replication TEM and in situ XRD studies, the effect of Zr(IV) ions on the evolution of mesostructure and morphologies of SBA-15 is summarized in Figure 8. In the early stage of assembly processs, it can be pictured that the threadlike P123 micelles coated with silica are formed after TEOS is introduced into the synthesis solution for about 10 min. As silica condensation proceeds, the disordered stuctures and aggregates of P123−silica nanocomposite materials are formed in the following 20−30 min. As the silicate further condensates around the P123 micelles, the micelles were stretched and aligned in 2D hexagonal arrangement. The short rods interconnect through the ends of the channels and form longer rods along the channeling direction as the reaction prolongs. On the other hand, the silicate condensation around the micelles was accelerated by the presence of Zr(IV) ions in the synthesis solution. The plate-shaped SBA-15 particles are a result of the quick silicate condensation which also terminates the possibility of interconnection between particles.

The Zr(IV) ions probably play two roles in the assembly process. One is the so-called salting-out effect, in which the highly solvated species reduce the cmc value of P123 triblock copolymer and probably also increase the local concentration of TEOS around P123 micelles. As a result, the hydrolysis and condensation of TEOS on P123 micelles are accelerated by adding Zr(IV) ions in synthesis solution. On the other hand, Zr(IV) species may interact with the hydrophilic PEO chains of P123 likely through dative bond. That interaction explains that Zr is mainly present on the surfaces of the pore walls and the observed expansion in the diameter of mesopores of the resultant platelet SBA-15.

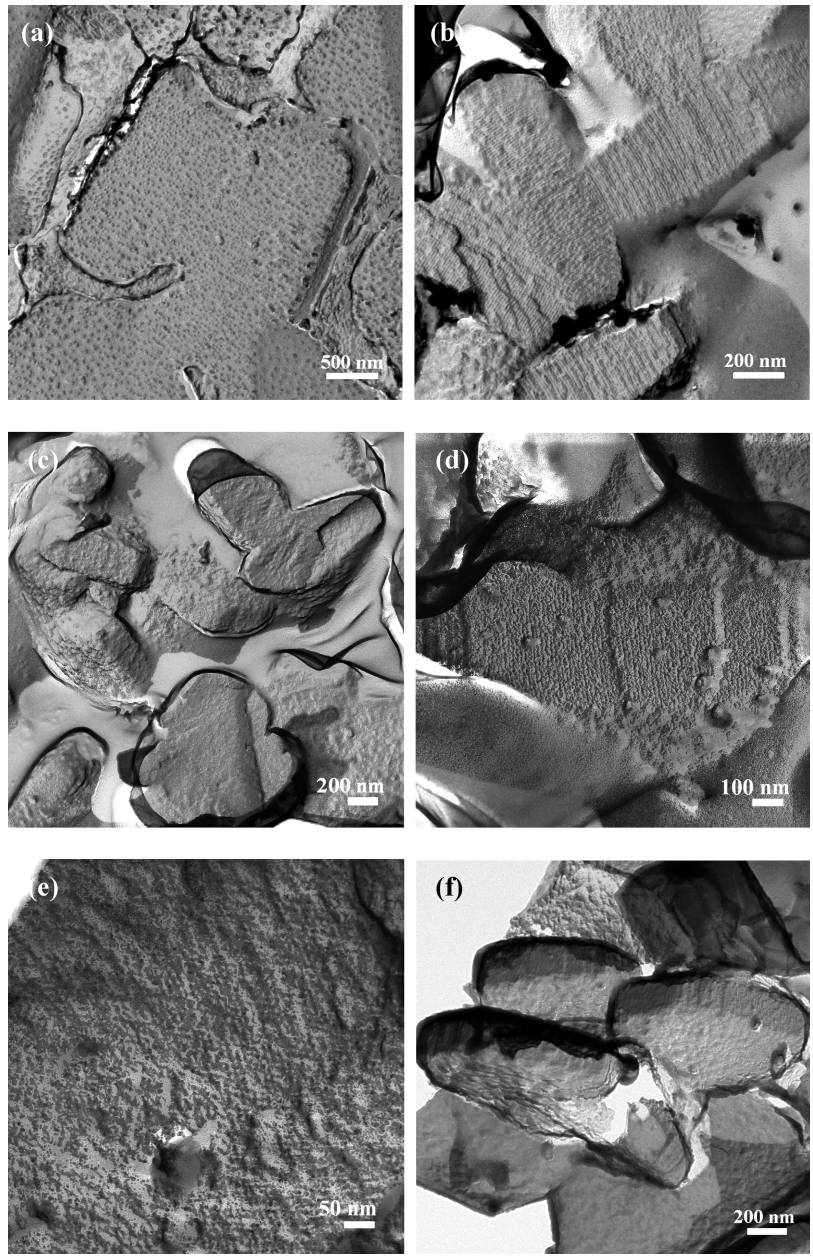

Figure 7. Freeze-fracture replication TEM images of SBA-15 synthesis solution containing Zr(IV) ions, taken after adding TEOS for (a) 30 min, (b) 40 min, (c, d) 1 h, (e) 1.5 h, and (f) 3 h.

The influence of organosilanes on the self-assembly process was also examined by in situ XRD. It was found that the process was seriously impeded if the organic silane and TEOS were mixed simultaneously in one pot (Figure 9a). That is especially pronounced when the organic moieties have lone pair electrons to form dative bonds with Zr(IV) ions or strongly interact with P123 micelles through hydrogen bonding. As a result, the precipitates without ordering pore arrangement were obtained.

It is well documented that prehydrolysis of TEOS is essential in order to obtain well-ordered SBA-15 materials with high loading of organic functional groups in one pot.[22–24] The organic functionalized SBA-15 with platelet morphology and short mesochannels were prepared with TEOS prehydrolysis for 1−4 h and the organosilane/TEOS ratios kept in 10 mol%. Although both freeze-fracture replication TEM and in situ XRD show that well ordered 2-D hexagonal structures are formed after TEOS is added for 40 min and 1.5 h with and without Zr(IV) ions, respectively, in situ XRD shows that the assembly processes are still perturbed by the introduction of organic silanes. Figure 9b shows that a broad diffraction at $2\theta \approx 0.61°$ was observed in several minutes in the acidic solution containing TEOS, P123, and Zr(IV). The peak grew stronger and sharper as the reaction progressed. When methyltriethoxysilane (MTES) was introduced into the synthesis gel after 1 h, the diffraction peak immediately weakened and moved toward higher angle. Nevertheless, the diffraction peak regained its intensity in the next 5 min and grew gradually without moving the position significantly. After TEOS was added for 1.5 h, the (110) and (200) diffraction peaks appeared at $2\theta \approx 1.13$ and 1.28°. These results indicate that the self-assembly of P123 micelles and TEOS is slightly perturbed by MTES, but

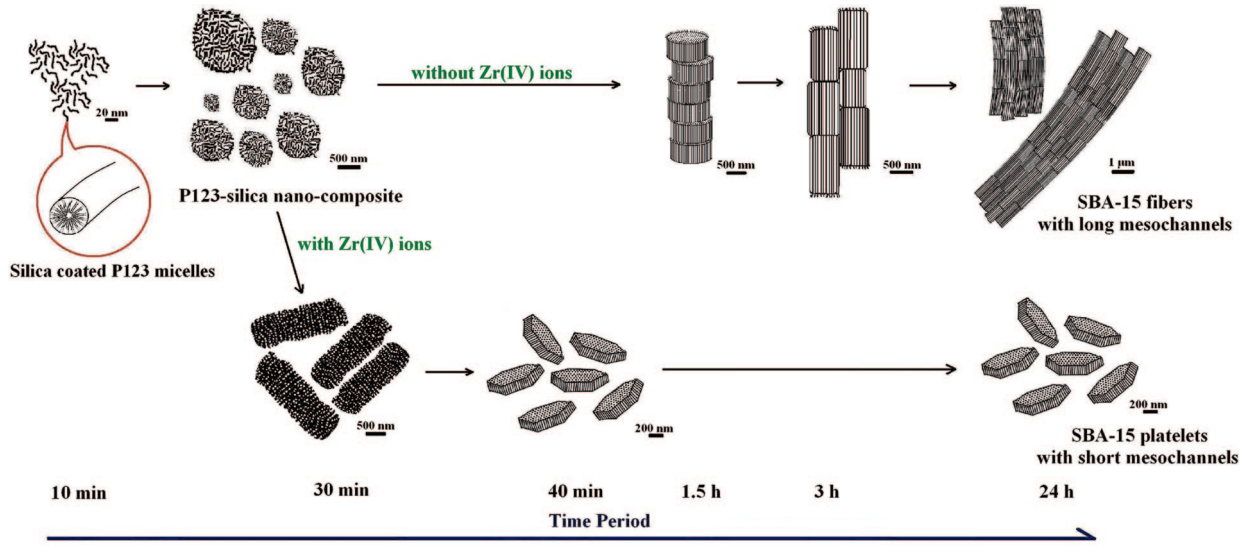

Figure 8. A schematic description of the effect of Zr(IV) ions on the evolution of mesostructures and morphologies of SBA-15 materials.

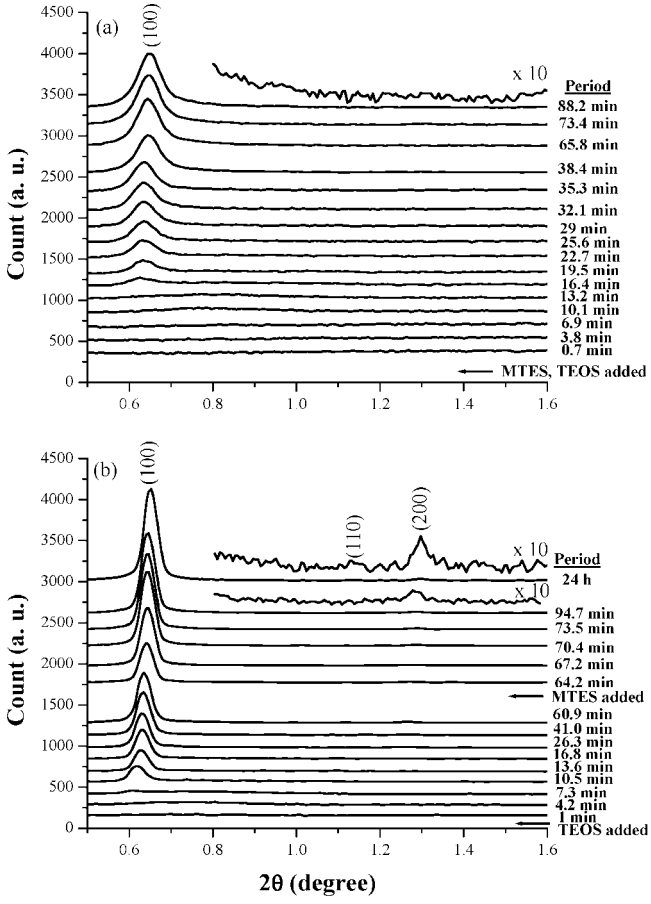

Figure 9. In situ XRD patterns using a synchrotron X-ray radiation source (λ = 1.33344 Å) of methyl-functionalized SBA-15 prepared with Zr(IV) ions: (a) no TEOS prehydrolysis, and (b) TEOS prehydrolysis for 1 h.

adding Zr(IV) species in the synthesis solution still dominates the rate of mesoporous silica formation.

The elemental analyses indicated that the FG/Si molar ratios in the solid products were similar to those introduced in the synthesis solutions (Table 1). Moreover, BJH analyses of the N_2 sorption isotherms showed that the organic functionalized SBA-15 platelets have smaller pore sizes but thicker pore walls than those of siliceous SBA-15 sample. These results infer that most of the organosilane precursors were incorporated onto the silica framework. In other words, the silicate condensation is still proceeding even the ordered pores are formed, and the reorganization of the silica framework can last longer than a day at reaction temperature of 35 °C.

Solid state ^{13}C and ^{29}Si NMR spectroscopes are the useful tools for characterization of the locally chemical environment of carbon and silicon elements in the mesoporous organosilica materials, such as the bonding of hydrocarbon and the condensation of organosiloxane and siloxane species.[22–27] Solid-state $^{13}C\{^1H\}$ cross-polarization and ^{29}Si MAS NMR spectra of the ethanol extracted platelet SBA-15 with various organic functionalities are shown in Figure 10. In the ^{13}C CP-MAS NMR spectra, the peak at −4.2 ppm corresponds to the C atom on the CH_3-Si group, two peaks at 128.2 and 133.7 ppm correspond to C atoms on the ph-Si groups, and three distinct peaks appeared at 9.6−11.7, 16.4−26.5 and 27.7−47.6 ppm corresponding to the carbon atoms of $Si-CH_2-CH_2-CH_2-$ groups in sequence from left to right for the propylene-containing functional groups.[22–27] Additional weak peaks at 24, 71, 74, and 76 ppm are attributed to the residual P123 template in the material.[25] The ^{13}C NMR spectra confirmed that the platelet SBA-15 materials are indeed incorporated with various organic functional groups

(22) Corriu, R. J. P.; Mehdi, A.; Reye, C.; Thieuleux, C.; Frenke, A.; Gibaud, A. *New. J. Chem.* **2004**, *28*, 156.
(23) Yang, Q.; Liu, J.; Yang, J.; Zhang, L.; Feng, Z.; Zhang, J.; Li, C. *Microporous Mesoporous Mater.* **2005**, *77*, 257.
(24) Liu, N.; Assink, R. A.; Smarsly, B.; Brinker, C. J. *Chem. Commun.* **2003**, 1146.
(25) (a) Yang, C. M.; Zibrowius, B.; Schuth, F. *Chem. Commun.* **2003**, 1772. (b) Yang, C. M.; Zibrowius, B.; Schmidt, W.; Schuth, F. *Chem. Mater.* **2004**, *16*, 2918.
(26) Margolese, D.; Melero, J. A.; Christainsen, S. C.; Chmelka, B. F.; Stucky, G. D. *Chem. Mater.* **2000**, *12*, 2448.
(27) (a) Wouters, B. H.; Chen, T.; Dewilde, M.; Grobet, P. J. *Microporous Mesoporous Mater.* **2001**, *44−45*, 453. (b) Luhmer, M.; d'Espinose, J. B.; Hommel, H.; Legrand, A. P. *Magn. Reson. Imaging* **1996**, *14*, 911.

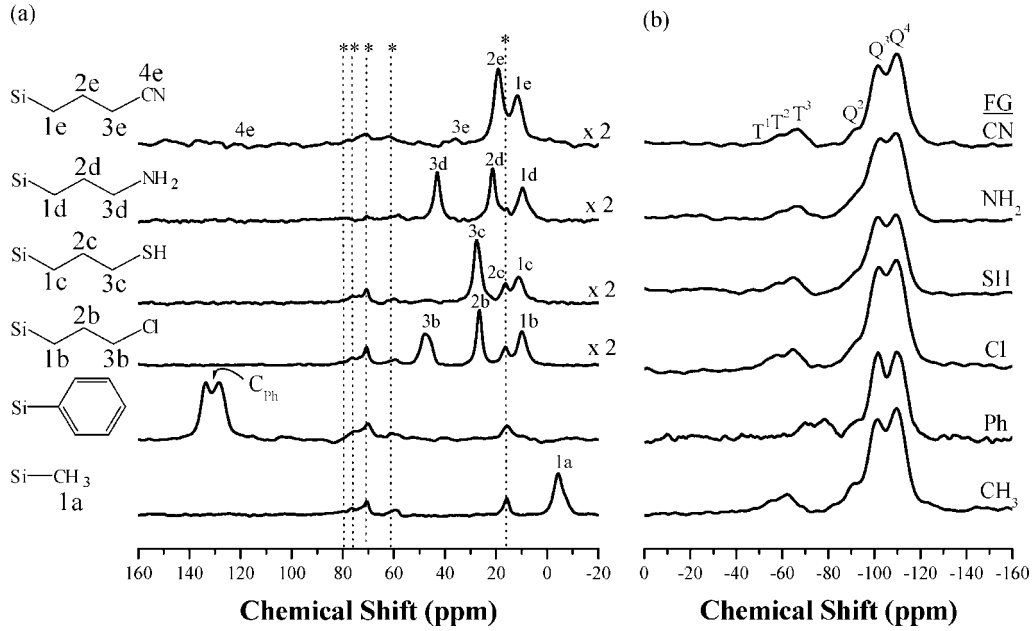

Figure 10. (a) Solid-state ^{13}C CP-MAS spectra and (b) ^{29}Si MAS NMR spectra of various extracted organic functionalized SBA-15 with platelet morphology and short mesochannels; Peaks labeled * correspond to carbon atoms from the P123 residue.

Table 2. Elemental Analyses and Textural Properties of Extracted Organic Functionalized SBA-15 of Fiber Shape and Long Mesochannels

		FG/Si							
functionality	PT[a](h)	gel	solid[b]	a_0(nm)	S_{BET}(m^2/g)	V_{Total}(cm^3/g)	Φ_P[c](nm)	PSD[d](nm)	W[e](nm)
none	0	0	0	10.6	802	0.95	5.7	0.6	4.9
CH_3	2	0.091	0.095	11.7	810	0.93	6.7	0.6	5.0
Ph	2	0.091	0.092	11.0	709	0.72	4.5	0.8	6.5
$(CH_2)_3Cl$	2	0.091	0.092	10.9	659	0.67	4.8	1.1	6.1
$(CH_2)_3SH$	2	0.091	0.087	11.6	598	0.60	4.5	1.1	7.1
$(CH_2)_3NH_2$	2	0.091	0.082	12.7	677	0.85	6.4	1.2	6.3
$(CH_2)_3CN$	2	0.091	0.095	12.1	720	0.79	5.8	0.9	6.3

[a] Prehydrolysis period. [b] FG/Si molar ratios are measured by CHNS elemental analysis. [c] Pore diameter. [d] Pore size distribution. [e] Wall thickness.

and the organic moieties are not decomposed during the preparation procedures.

The ^{29}Si MAS NMR spectra of the functionalized SBA-15 platelets all have three distinct resonance peaks in upfield corresponding to Q^n ($Q^n = Si(OSi)_n(OH)_{4-n}$, $n = 2-4$; Q^4 at -110 ppm, Q^3 at -101 ppm, and Q^2 at -91 ppm) and three weaker peaks in downfield assigned to T^m (T^m=$RSi(OSi)_m(OH)_{3-m}$, $m = 1-3$). The appearance of T^m peaks confirms that the organic silane is incorporated as a part of the silica wall structure. The (Q^4/Q^2+Q^3) values of organic functionalized SBA-15 platelets are in 1.10−1.24, slightly lower than 1.28−1.36 for siliceous SBA-15,[6,27,28] implying that the condensation of the silica framework is less complete in the presence of organic silanes. The $\Sigma T^m/\Sigma Q^n$ values are around 0.086−0.097, which are consistent with the results of elemental analyses.

Inorganic salts are commonly added into the synthesis solutions in order to obtain well-ordered SBA-15.[10,19b,c,28–32] The pore ordering and textural properties of the organic functionalized SBA-15 were indeed markedly improved when 1.5 M NaCl was added (Table 2). However, SEM images show that the morphology of the resultant SBA-15 materials is fiberlike aggregates with about 500 nm in diameter and 10 μm in length (see the Supporting Information). TEM images show that the mesochannels are aligned along the length of fibers, which is longer than 10 μm.

The uptakes of new coccine dye (Supporting Information) and octadecane on organic functionalized SBA-15 materials with platelet and fiber morphologies are compared and summarized in Table 3. The uptakes of new coccine on conventional SBA-15 materials are all slightly lower than those over platelet materials. The differences are enlarged when the materials contain organic functional groups, especially phenyl and cyanopropyl groups. It is also noticeable that the absorption capacities of aminopropyl-functionalized SBA-15 toward new coccine are much higher than those over other materials, probably because of the strong hydrogen-bond interaction between the anchored aminopropyl and the sulfate groups on the dye. The adsorption rates of new coccine dye on aminopropyl-functionalized SBA-15

(28) (a) Chen, S. Y.; Cheng, S. *Stud. Surf. Sci. Catal.* **2005**, *156*, 89. (b) Chen, S. Y.; Cheng, S. *Chem. Mater.* **2007**, *19*, 3041.
(29) (a) Yu, C.; Tian, B.; Fan, J.; Stucky, G. D.; Zhao, D. *J. Am. Chem. Soc.* **2002**, *124*, 4556. (b) Yu, C.; Fan, J.; Tian, B.; Zhao, D.; Stucky, G. D. *Adv. Mater.* **2002**, *14*, 1742.
(30) (a) Das, D.; Tsai, C. M.; Cheng, S. *Chem. Commun.* **1999**, 473. (b) Chen, S. Y.; Jang, L. Y.; Cheng, S. *J. Phys. Chem. B* **2006**, *110*, 11761.
(31) Flodstrom, K.; Alfredsson, V.; Kallrot, N. *J. Am. Chem. Soc.* **2003**, *125*, 4402.
(32) Guo, W.; Park, J. Y.; Oh, M. O.; Jeong, H. W.; Cho, W. J.; Kim, I.; Ha, C. S. *Chem. Mater.* **2003**, *15*, 2295.

Table 3. Adsorption Amounts of New Coccine and Octadecane over Extracted Organic Functionalized SBA-15 with Short and Long Mesochannels[a]

	uptake of new coccine (mmol/g)		uptake of octadecane(mmol/g)	
functionality	long mesochannels	short mesochannels	long mesochannels	short mesochannels
none	0.34	0.37	0.40	1.10
CH_3	0.65	0.93	7.83	8.04
Ph	0.71	1.18	5.90	7.69
$(CH_2)_3Cl$	0.73	0.93	5.00	7.77
$(CH_2)_3SH$	1.11	1.35	5.49	6.19
$(CH_2)_3NH_2$	14.3	15.4	2.44	5.25
$(CH_2)_3CN$	0.77	1.23	5.00	5.75

[a] Adsorption experiments were carried out at RT for 1 day; new coccine in ethanol, octadecane in hexane.

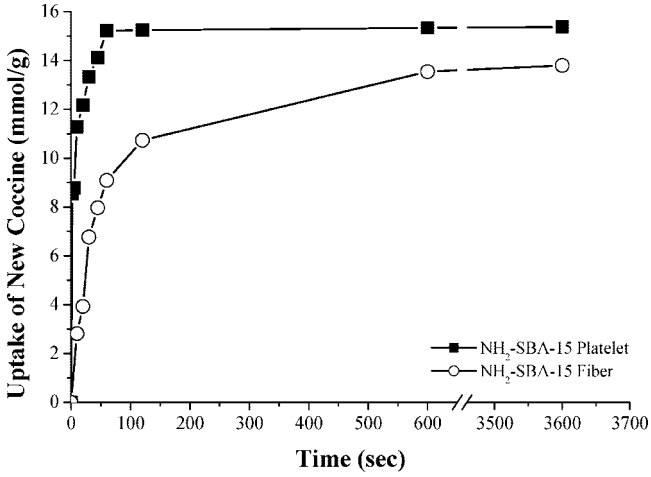

Figure 11. Uptakes of new coccine as a function of adsorption period at RT over extracted $NH_2(CH_2)_3$-functionalized SBA-15 with short (■) and long (○) mesochannels.

with short and long mesochannels were compared in order to understand the effect of pore length on the molecular diffusivity through the channels. Figure 11 shows that it takes ca. 10 min for the adsorption of new coccine dye to reach equilibrium on the fiber material, whereas it takes only 1 min on the platelet material. These results demonstrate that the short mesochannels facilitate the diffusion of the bulky dye molecules through the channels. Moreover, the higher uptake of new coccine dye by SBA-15 with platelet morphology and short mesochannels is attributed to the smaller possibility of pore-blockage in comparison to that with long mesochannels.

Conclusions

Large pore SBA-15 silica of platelet shape and very short mesochannels in 150−350 nm was developed by introducing a small amount of Zr(IV) ions in the synthesis solution. The in situ XRD and freeze-fracture replication cryo-TEM are powerful techniques to study the self-assembly process of mesoporous materials. The platelet SBA-15 with short mesochannels was formed due to the fast self-assembly of P123 micelles and TEOS accelerated by the Zr(IV) ions in the synthesis solution. With the aid of TEOS prehydrolysis, this synthesis route could be easily extended to prepare various organic functionalized SBA-15 materials with platelet morphology and short mesochannels. These materials are superior to the conventional SBA-15 of rod or fiber morphologies in facilitating molecular diffusion and less possibility of pore blockage when used in the sorption or reactions of bulky molecules.

Acknowledgment. This work was supported by National Science Council, the Ministry of Education, Taiwan, and Taiwan Textile Research Institute. S.Y.C. thanks C.-W. Lu of the Instrumentation Center, National Taiwan University, for CHNS analysis experiments, and C.-N. Ke of National Tsing-Hua University for the ICP-AES experiments.

Supporting Information Available: Figures S1−S4 and additional experimental details (PDF). This material is available free of charge via the Internet at http://pubs.acs.org.

CM703500C